Image Processing with Complex Daubechies Wavelets

Article *in* Journal of Mathematical Imaging and Vision · June 1997

DOI: 10.1023/A:1008274210946 · Source: DBLP

1 author:

jean-marc Lina
École de Technologie Supérieure
193 PUBLICATIONS **4,928** CITATIONS

Image Processing with Complex Daubechies Wavelets

J.-M. Lina*
Centre de Recherches Mathématiques, Univ. de Montréal
C.P. 6128 Succ. Centre-Ville, Montréal(Québec), H3C 3J7, Canada
and
Atlantic Nuclear Services Ltd., Fredericton, New Brunswick, E3B 5C8, Canada

Abstract

Analyses based on Symmetric Daubechies Wavelets (SDW) lead to complex-valued multiresolution representations of real signals. After a recall of the construction of the SDW, we present some specific properties of these new types of Daubechies wavelets. We then discuss two applications in image processing: enhancement and restoration. In both cases, the efficiency of this multiscale representation relies on the information encoded in the phase of the complex wavelet coefficients.

1. INTRODUCTION

Many current investigations in mathematical imaging consist in finding the optimal representation to perform specific enhancements by extracting the relevant information contained in an empirical signal. This question of *representation*, present in many fields of applied mathematics and physics, is indeed the cornerstone of the pionnering work of D. Marr in vision[1]. The "primal sketch" of an image he proposed was based on the multiscale edge representation obtained through the action of some operators of different sizes. More specifically, Marr and Hildreth[2] argued that the convolution of the image with the filter associated with the Laplacian of the two dimensional Gaussian at different scales constitutes the most satisfactory representation. Such a representation identifies edges with the *zero-crossings* of the filtered image. Physiological experiments[1] gave credit to this model of vision generally known as the "Marr conjecture". In a more computational approach to edge detection proposed by Canny[3], edges are located at the *local extrema* of the convolutions of the image with the directional first order derivatives of some smoothing function (*e.g.* a Gaussian kernel). Unlike the zero-crossing technique, the Canny's edge detector characterizes the strength of the discontinuities in the image intensity. The synthesis of those two approaches is due to Mallat and Zhong[4,5] who demonstrated that *zero-crossings* and *local extrema* are unified in a single mathematical framework: the wavelet theory of frames. They further established an iterative algorithm to restore the original signal from these sparse representations. The aim of the present work is to show that similar ideas can be developped with *orthogonal multiresolution bases with compact support* provided we use the symmetric Daubechies wavelets[6,7].

Being complex-valued, the symmetric Daubechies multiresolution analyses did not receive much attention from the signal processing community since the resulting representation of a real field, such as an image, is a redundant expansion with complex-valued coefficients. Needless to say, this is also true with the Fourier transform; however, the reality condition is rather trivial and establishes a simple identity between the Fourier modes. The present work investigates the same kind of relationship between the complex wavelet coefficients: on the basis of comparison with the standard real Daubechies analyses, we show that the "natural

*e-mail: lina@crm.umontreal.ca

redundancy" given by the complex Daubechies analyses of a real field provides a "dual representation" combining zero-crossings and local extrema. In fact, this result relies on the existence of "hidden" differential operators underlying the structure of some complex Symmetric Daubechies Wavelets (SDW). This result has interesting potential applications in numerical simulations[8] and signal processing[9,10].

Pursuing the analogy with Fourier representation, we can also wonder where the essential information of a signal is located in the complex wavelet coefficients. In the context of Fourier analysis, this point has been discussed by many authors who investigated the "importance of the phase in signals"[11,12,13]. In the same way, most of the information is encoded in the phase of the wavelet coefficients and we describe a "phase-only wavelet synthesis" algorithm that restore most of the signal from a "shrunk representation" as suggested by many authors[14,15].

The paper is organized as follows. Section 2 briefly describes the basics of the multiresolution analyses and the SDW solutions following the standard factorisation approach. More details and results can be found in Ref.[7,10]. In Section 3, the SDW are discussed in terms of parametrized filter banks. In Section 4, we describe the differential operators underlying some complex symmetric Daubechies multiresolution bases. The consequences in two dimensions and application to edge enhancements are discussed in Section 5. Denoising and "phase reconstruction" are finally presented in Section 6. Conclusion will follow.

Notation: The derivatives and partial derivatives are denoted by a superscript as in Eq.(14) and by $\partial_x^m f$, respectively. Complex conjugation of z is written $\overline{z}$.

2. SYMMETRIC DAUBECHIES WAVELETS

A multiresolution analysis of $L^2(\mathbb{R})$ is a sequence of closed subspaces $V_j \subset L^2(\mathbb{R})$ such that

$$V_j \subset V_{j+1}, \quad \bigcap_j V_j = \{0\}, \quad \overline{\bigcup_j V_j} = L^2(\mathbb{R}), \tag{1a}$$

$$f(x) \in V_0 \Leftrightarrow f(x-1) \in V_0, \quad f(x) \in V_j \Leftrightarrow f(2x) \in V_{j+1} \tag{1b}$$

A scaling function $\varphi \in V_0$ with unit integral exists such that $\{\varphi_{0,k}(x) \equiv \varphi(x-k), k \in \mathbb{Z}\}$ is an orthonormal basis of V_0 and, consequently, the set of functions

$$\varphi_{j,k}(x) = 2^{\frac{j}{2}} \varphi(2^j x - k) \tag{2}$$

is an orthonormal basis of the space V_j. Since $\varphi \in V_0 \subset V_1$, a sequence of complex-valued coefficients a_k exists such that $\sum a_k = 1$ and

$$\varphi(x) = 2 \sum_k a_k \ \varphi(2x-k) \tag{3}$$

Multiresolution aims to decompose $L^2(\mathbb{R})$ as

$$L^2(\mathbb{R}) = V_{j_0} \oplus \sum_{j \geq j_0} W_j \tag{4}$$

where the spaces W_j are defined as the orthogonal complement of V_j in V_{j+1}: $V_{j+1} = V_j \oplus W_j$. For a given scale j, the space W_j is generated by the set of orthonormal wavelets $\psi_j(x) = 2^{\frac{j}{2}} \psi(2^j x)$ associated with the multiresolution analysis. Since $\psi \in W_0 \subset V_1$, a sequence of complex-valued coefficients b_k exists such that:

$$\psi(x) = 2 \sum_k b_k \ \varphi(2x-k) \tag{5}$$

The choice $b_k = (-1)^k \overline{a}_{1-k}$ ensures that the set $\{\psi_j(x - 2^{-j}k), k \in \mathbb{Z}\}$ is an orthonormal basis of W_j.
In general, a field with finite energy will be "empirically known" at some scale and approximated in some $V_{j_{max}}$,

$$f(x) = \sum_k c_k^{j_{max}} \, \varphi_{j_{max},k}(x) \tag{6}$$

The discrete multiresolution analysis of f consists in the computation of the coefficients of the expansion

$$f(x) = \sum_k c_k^{j_0} \, \varphi_{j_0,k}(x) + \sum_{j=j_0}^{j_{max}-1} \sum_k d_k^j \, \psi_{j,k}(x) \tag{7}$$

where j_0 is a given low resolution scale. The coefficients in the previous expansion are computed through the orthogonal projection of the field over the multiresolution basis:

$$c_k^j = \langle \varphi_{j,k} | f \rangle, \qquad d_k^j = \langle \psi_{j,k} | f \rangle \tag{8}$$

Using the previous definition, we have the well-known *fast wavelet decomposition algorithm* composed with the low-pass projection $V_j \to V_{j-1}$ and the high-pass projection $V_j \to W_{j-1}$:

$$c_n^{j-1} = \sqrt{2} \sum_k \bar{a}_{k-2n} c_k^j, \qquad \text{and} \qquad d_n^{j-1} = \sqrt{2} \sum_k \bar{b}_{k-2n} c_k^j \tag{9}$$

Conversely, any elements of V_{j-1} and of W_{j-1} can combine to give a unique vector in V_j; this reconstruction is expressed by the inverse fast wavelet transform:

$$c_n^j = \sqrt{2} \sum_k a_{n-2k} c_k^{j-1} + \sqrt{2} \sum_k b_{n-2k} d_k^{j-1} \tag{10}$$

The Symmetric Daubechies Wavelets are subject to the following constraints:
(*i*) Compactness of the support of φ: We require that φ (and consequently ψ) has a compact support inside the interval $[-J, J+1]$ for some integer J that is, $a_k \neq 0$ for $k = -J, -J+1, \ldots, J, J+1$.
(*ii*) Orthogonality of the $\varphi(x-k)$: This condition defines in a large sense the Daubechies wavelets. Defining the polynomial

$$F(z) = \sum_{n=-J}^{J+1} a_n \, z^n, \quad \text{with } F(1) = 1 \tag{11}$$

where z is on the unit circle, $|z| = 1$, the orthonormality of the set $\{\varphi_{0,k}(x), k \in \mathbb{Z}\}$ can be stated through the following identity

$$P(z) - P(-z) = z \tag{12}$$

where the polynomial $P(z)$ is defined as

$$P(z) = zF(z)\overline{F(z)} \tag{13}$$

(*iii*) Accuracy of the approximation (6): To maximize the regularity of the functions generated by the scaling function φ, we require the vanishing of the first J moments of the wavelet or, in terms of the polynomial (11),

$$F'(-1) = F''(-1) = \ldots = F^{(J)}(-1) = 0 \tag{14}$$

The usual Daubechies wavelets[16] are the real polynomial solutions of Eqs.(12) and (14). They differ from each other through their degree of symmetry and, in general, the standard Daubechies wavelet (DAUBn) is the "least asymmetric" solution ($n = 2J + 2$ being the length of the filters).

(*iv*) Symmetry: This condition on the filter,*i.e* $a_k = a_{1-k}$, can be written as

$$F(z) = z\,F(z^{-1}) \tag{15}$$

As anticipated by Lawton[17], only *complex-valued* solutions of φ and ψ, under the four above constraints, can exist, and for J even, only. The first solutions (from $J = 0$ to $J = 8$) were described in Ref.[7] by using the parametrized solutions of Eqs. (12), (14) and (15). The solutions have also been investigated in the spirit of the original Daubechies approach, *i.e.* by inspection of the roots of some so-called "valid polynomial" that satisfies Eq.(12). Such a polynomial is defined by

$$P_J(z) = \left(\frac{1+z}{2}\right)^{2J+2} p_J(z^{-1}) \tag{16}$$

where

$$p_J(z) = \sum_{j=0}^{2J} r_j (z+1)^{2J-j}(z-1)^j, \text{ with } \begin{cases} r_{2j} = (-1)^j 2^{-2J}\binom{2J+1}{j}, \\ \\ r_{2j+1} = 0 \end{cases}, \ j = 0, 1, \ldots, J \tag{17}$$

Straightforward algebra shows that $P_J(z)$ does satisfy Eq.(12).

The $2J$ roots of $p_J(z)$ display obvious symmetries: the conjugate and the inverse of a root are also roots; furthermore, no root is of unit modulus. If we denote by $x_{k=1,2,\ldots,J}$ the roots inside the unit circle ($|x_k| < 1$) and $\bar{x}_k = x_{J+1-k}$, then

$$p_J(z) = \prod_{k=1}^{J} \left(\frac{z - x_k}{1 - x_k}\right) \prod_{k=1}^{J} \left(\frac{z - \bar{x}_k^{-1}}{1 - \bar{x}_k^{-1}}\right) \tag{18}$$

and the low-pass filter $F(z)$ can be written as:

$$F(z) = \left(\frac{1+z}{2}\right)^{1+J} p(z^{-1}), \text{ with } p(z) = \prod_{m \in R} \left(\frac{z - x_m}{1 - x_m}\right) \prod_{n \in R'} \left(\frac{z - \bar{x}_n^{-1}}{1 - \bar{x}_n^{-1}}\right) \tag{19}$$

The polynomial $p(z)$ is defined through some particular roots of $p_J(z)$; R, R' are two arbitrary subsets of $\{1, 2, 3, \ldots, J\}$. The spectral factorization of $P_J(z)$, *i.e.* $P_J(z) = zF(z)\overline{F}(z)$ implies $p_J(z) = z^J p(z^{-1})\overline{p(z)}$ and leads to the following constraint on R and R':

$$k \in R \Longleftrightarrow k \notin R' \tag{20}$$

This selection of roots fulfills the conditions *(i),(ii)* and *(iii)*. In her seminal work[16], Daubechies investigates all the *real* solutions for a_k derived from the condition (20). This amounts to restrict the definition (20) and to consider the rule

$$k \in R \Longleftrightarrow J - k + 1 \in R \text{ and } k \notin R' \tag{21}$$

For instance, $R = \{1, 2, 3, \ldots, J\}$ and $R' = \emptyset$ corresponds to the DAUBn solution with $n = 2J + 2$. The symmetry condition *(iv)* defines an other subset of solutions of Eq.(20). It corresponds to the following rule of selection for the roots

$$k \in R \Longleftrightarrow J - k + 1 \in R' \text{ and } k \notin R' \tag{22}$$

We first notice that "reality" (rule (21)) and symmetry (rule (22)) are incompatible: all the symmetric Daubechies wavelets are complex valued. For any even value of J, Eq.(22) defines a subset of $2^{\frac{J}{2}}$ solutions in the original set of "orthogonal compactly supported regular wavelets" (2^J elements, complex or real). Notice that a complex conjugate of a scaling function is also a scaling function.

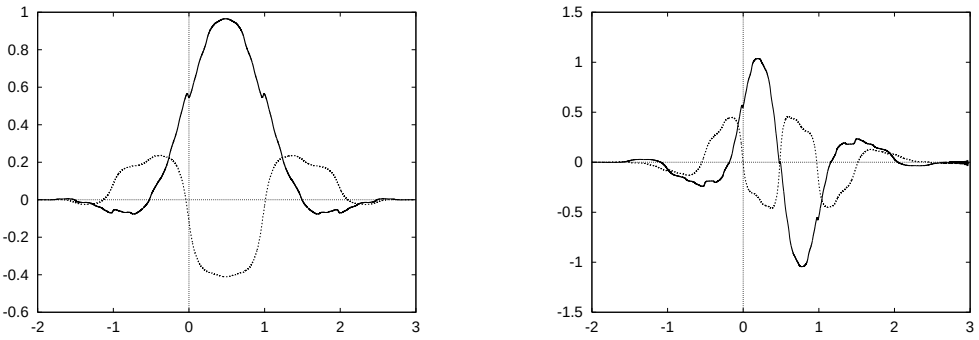

Figure 1: The complex scaling function φ for J=2. Right: The complex wavelet ψ for J=2. (Imaginary part in dashed line).

The complex scaling function and wavelet will be written as

$$\varphi(x) = h(x) + i\, g(x) \quad \text{and} \quad \psi(x) = w(x) + i\, v(x) \tag{23}$$

where h, g, w and v are all real functions. In the present work, we will consider a particular family of solutions, the so-called SDWJ Daubechies wavelets, that correspond to the following selection of roots:

$$R = \{1, 3, 5, \ldots, 2k+1, \ldots, J-1\}, \quad R' = \{2, 4, \ldots, 2k, \ldots, J\} \tag{24}$$

that clearly satisfies the constraints (22). For $J = 2$, the unique solution (SDW2) is shown on Fig.1. The two symmetric solutions for $J = 4$ are shown on Fig.2 and Fig.3; the SDW4 solution corresponding to the definition (24) is shown on Fig. 2. Finalyy, Figs. 4 display the four real functions h, g, w and v of SDW6. The filter coefficients $\sqrt{2}\, a_k$ for SDW2, SDW4 and SDW6 are:

k	*J=2*	*J=4*	*J=6*
1	$0.662912 + 0.171163i$	$0.643003 + 0.182852i$	$0.633885 + 0.179835i$
2	$0.110485 - 0.085581i$	$0.151379 - 0.094223i$	$0.171512 - 0.094452i$
3	$-0.066291 - 0.085581i$	$-0.080639 - 0.117947i$	$-0.086478 - 0.130859i$
4	0.000000	$-0.017128 + 0.008728i$	$-0.030746 + 0.014044i$
5	0.000000	$0.010492 + 0.020590i$	$0.017651 + 0.037601i$
6	0.000000	0.000000	$0.003238 - 0.001300i$
7	0.000000	0.000000	$-0.001956 - 0.004869i$

To conclude this section, we recall that the bi-dimensional multiresolution analysis is built from the tensor product of two multiresolution spaces V_i. We thus have one scaling function $\varphi(x)\varphi(y)$ complemented with three wavelets $\psi(x)\varphi(y), \varphi(x)\psi(y)$ and $\psi(x)\psi(y)$. We will write these complex-valued basis functions as

$$\Phi(x,y) = \varphi(x)\varphi(y) = \Theta(x,y) + i\,\Psi(x,y), \tag{25}$$

$$\Psi^0(x,y) = \psi(x)\psi(y) = \xi_0(x,y) + i\,\zeta_0(x,y), \tag{26}$$

$$\Psi^1(x,y) = \psi(x)\varphi(y) = \xi_1(x,y) + i\,\zeta_1(x,y), \tag{27}$$

$$\Psi^2(x,y) = \varphi(x)\psi(y) = \xi_2(x,y) + i\,\zeta_2(x,y), \tag{28}$$

and expansions like (6) and (7) now generalize in two dimensions as

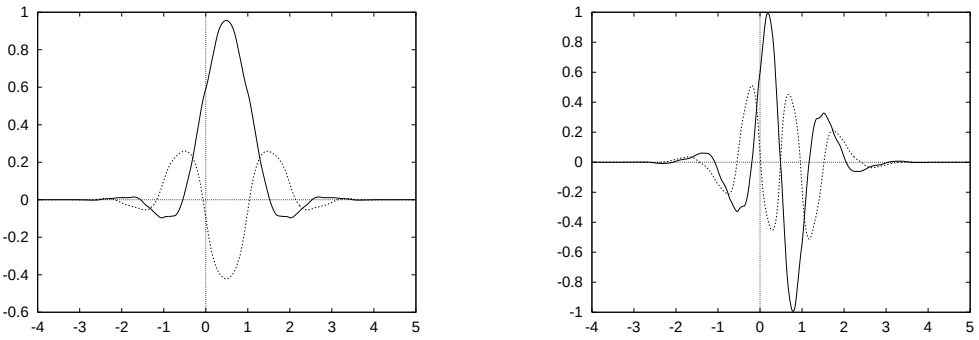

Figure 2: SDW4: The complex scaling function φ (left) and the complex wavelet ψ (Imaginary part in dashed line).

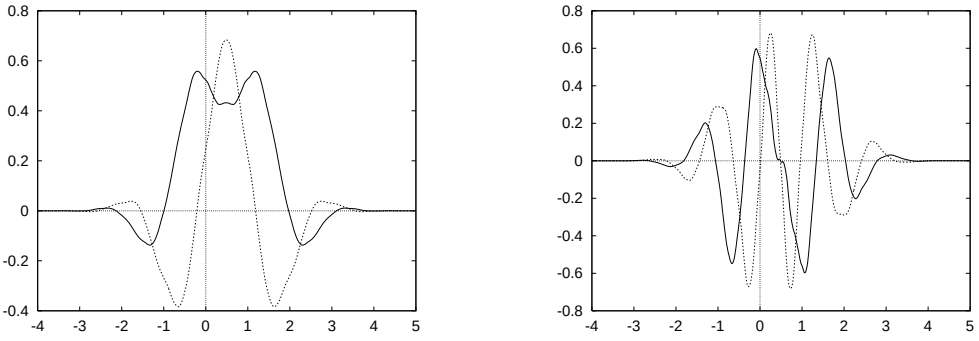

Figure 3: Complex Daubechies scaling function φ (left) and wavelet ψ (right) for J=4. (Imaginary part in dashed line).

$$I(x,y) = \sum_{m,n} c_{m,n}^{j_{max}} \Phi_{j_{max},m,n}(x,y) \tag{29}$$

$$= \sum_{k_1,k_2} c_{k_1,k_2}^{j_0} \Phi_{j_0,k_1,k_2}(x,y) + \sum_{i=0}^{2} \sum_{j=j_0}^{j_{max}-1} \sum_{k_1,k_2} d_{j,k_1,k_2}^{i} \Psi_{j,k_1,k_2}^{i}(x,y) \tag{30}$$

where $\Phi_{j,k_1,k_2}(x,y) = 2^j \Phi(2^j x - k_1, 2^j y - k_2)$ and $\Psi_{j,k_1,k_2}^{i}(x,y) = 2^j \Psi^i(2^j x - k_1, 2^j y - k_2)$ span the spaces V_j and W_j^i respectively. In the sequel, we denote by $\mathcal{W}_N$ the wavelet transform

$$\{c_{m,n}^{j_{max}}\} \xrightarrow{\mathcal{W}_N} \{c_{m,n}^{j_{max}-N}, \mathbf{d}_{j_{max}-N,m,n}, \mathbf{d}_{j_{max}-2,m,n}, \ldots \mathbf{d}_{j_{max}-1,m,n}\} \tag{31}$$

where $\mathbf{d} = (d^0, d^1, d^2)$.

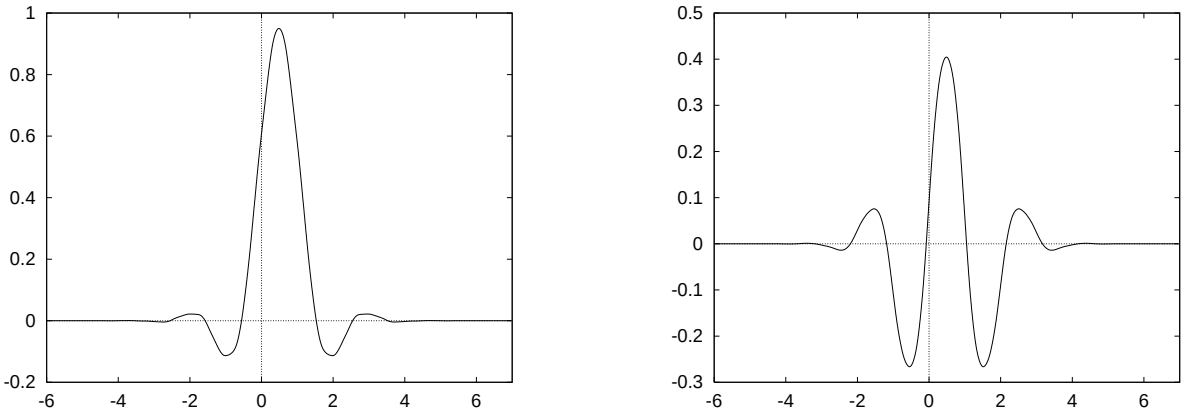

Figure 4: SDW6: $\varphi = h(x) + ig(x)$. Left: $h(x)$. Right: $g(x)$.

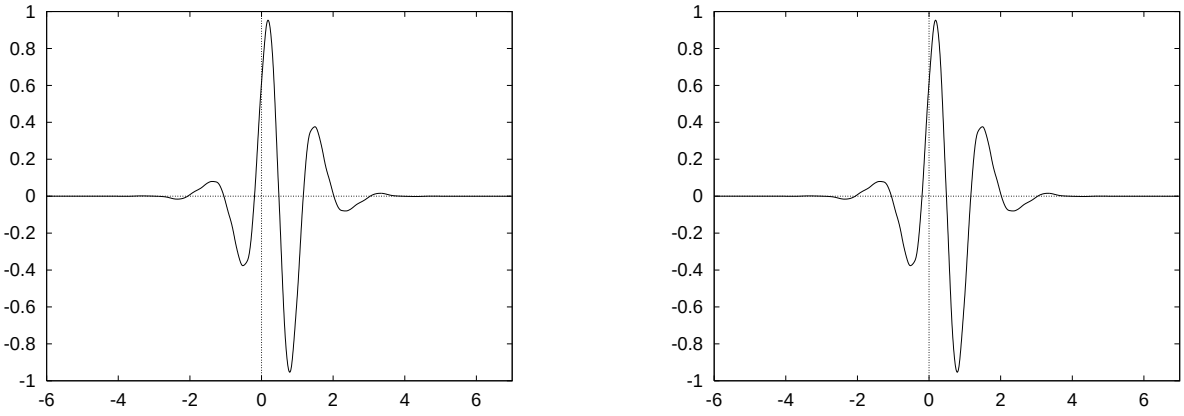

Figure 5: SDW6: $\psi = w(x) + iv(x)$. Left: $w(x)$. Right: $v(x)$.

3. PARAMETRIZATION OF THE SYMMETRIC DAUBECHIES FILTER BANKS

A few years ago, D. Pollen[18] studied the correspondance between the orthonormal multiresolution analysis (with compact supported scaling function) and the element of the group of the two by two matrices of the form

$$G(z) = \begin{pmatrix} u(z) & v(z) \\ -\overline{v(z)} & \overline{u(z)} \end{pmatrix}, \text{ with } |det(G(z))| = 1 \tag{32}$$

where z is still a complex variable on the unit circle and $u(z)$, $v(z)$ are polynomials in $\mathbb{C}[z, z^{-1}]$. Defining the unit vector

$$c(z) = \frac{1}{\sqrt{2}} \begin{pmatrix} z \\ -1 \end{pmatrix}, \tag{33}$$

Pollen has shown that

$$F(z) = \langle c(1)|G(z^2)|c(z)\rangle \tag{34}$$

solves the orthogonality condition expressed by Eqs.(12) and (13) if and only if $G(z)$ is *unitary* with $G(1) = 1$, *i.e.* $G(z)$ element of the group $SU_I(2,\mathbb{C}[z, z^{-1}]$. Such element can be factorized in a unique way:

$$G(z) = G_{\nu_1}(z)G^\dagger_{\nu_2}(z)G_{\nu_3}(z)G^\dagger_{\nu_4}(z)\ldots G_{\nu_{J-1}}(z)G^\dagger_{\nu_J}(z) \tag{35}$$

where $G_\nu(z)$ is an element of $SU_I(2,\mathbb{C}[z, z^{-1}]$ labelled with a complex parameter ν:

$$G_\nu(z) = \begin{pmatrix} u_\nu(z) & v_\nu(z) \\ -\overline{v_\nu(z)} & \overline{u_\nu(z)} \end{pmatrix} \text{ with } \begin{cases} u_\nu(z) = 1 + \frac{\nu\overline{\nu}}{1+\nu\overline{\nu}}(z^{-1} - 1) \\ v_\nu(z) = \frac{\nu}{1+\nu\overline{\nu}}(z - 1) \end{cases} \tag{36}$$

For $J = 1$, the expansion of $F(z)$ defined as Eq.(33) leads to the following four parametrized scaling coefficients

$$a_{-1} = \frac{\overline{\nu}(\nu + 1)}{2(1 + \nu\overline{\nu})},\ a_0 = \frac{(1 + \nu)}{2(1 + \nu\overline{\nu})},\ a_1 = \frac{(1 - \overline{\nu})}{2(1 + \nu\overline{\nu})},\ a_2 = \frac{\nu(\overline{\nu} - 1)}{2(1 + \nu\overline{\nu})} \tag{37}$$

For $\nu \in \mathbb{R}$, we recognize the $J = 1$ solution already mentioned in the early works of Daubechies[16]. We further notice that symmetry of the filter (37) is only possible for *purely imaginary complex* parameter ν. In fact, this observation can be generalized[7]: the scaling coefficients of any symmetric orthogonal multiresolution analysis can be computed from the definition (34), the factorization (35) and a set of complex parameters $\nu_n = ir_n$, $n = 1, \ldots, J$ where $r_n \in \mathbb{R}$. Let us emphasize that, at this point, no vanishing moments of the wavelet have been requested. For a given value of J, the vanishing moments conditions expressed by Eq.(14) define a finite set of parameters $\{r_n, n = 1, \ldots, J\}$. As studied in Ref.[7], this set which is empty when J is odd, contains $2^{\frac{J}{2}}$ solutions for J even. For instance, the $J = 2$ symmetric solution displayed in the previous section is given by $\nu_1 = i\sqrt{\frac{5}{3}}$, $\nu_2 = i\sqrt{\frac{3}{5}}$.

4. SOME PROPERTIES OF THE SYMMETRIC DAUBECHIES WAVELETS

All the Symmetric Daubechies Wavelets share the usual properties of the standard *real* Daubechies bases. In this section, we show that SDW have an unexpected analytic structure that relates real and complex part of the basis functions[10].

Using the Fourier representation of real functions $g(x)$, $h(x)$, $v(x)$ and $w(x)$ that define $\varphi(x)$ and $\psi(x)$, it can be shown that, for the first values of J (say $J < 12$), the complex scaling function and the wavelet of

the SDWJ multiresolution analysis can be written as

$$\begin{cases} \varphi(x) \simeq (1 + i\alpha\partial_x^2)\, h(x) \\ \\ \psi(x) \simeq (1 + i\kappa + i\beta\partial_x^2)\, w(x) \end{cases} \tag{38}$$

Those identities are verified on the frequency domain defined by the sampling rate of the analysed signal. In other words, those two identites are verified in the interval $[0, \pi]$ (with a sampling step renormalized to unity) when they are written in the Fourier representation.
For $J > 10$, higher derivative terms in $g(x)$ become non negligible. Of course, the two real functions $h(x)$ and $w(x)$ are the genuine scaling function and the true wavelet *only* in the cases of the real Daubechies multiresolution analyses ($\alpha = \beta = \kappa = 0$). In the complex case, $h(x)$ (the real part of the scaling function) and $w(x)$ (the real part of the wavelet) are still endowed with interesting properties. Indeed, $h(x)$ is a good interpolating function since we can easily verify that

$$\int dx\, h(x) = 1 \ \text{ and } \int dx\, h(x)\, (x - \frac{1}{2})^m = 0 \quad \text{for} \quad m = 1, 2 \text{ and } 3 \tag{39}$$

Let us recall that, in the early age of the Daubechies wavelets, the introduction of vanishing moments for the scaling function led to the construction of the well-known *coiflets*. Let us mention that $w(x)$, that is an "admissible wavelet" with J vanishing moments, can be well approximated with $\partial_x^{J+1} h(x)$ up to some multiplicative factor that can be computed. The parameters α, β and κ in (38) can be also computed directly from the filters coefficients a_k by using the first non vanishing momentum of $\varphi(x)$ and $\psi(x)$. Denoting by

$$\gamma_i = \int \bar{\varphi}(x)\, x^i dx, \quad \Gamma_i = \int \bar{\psi}(x)\, x^i dx \tag{40}$$

we have

$$\gamma_i = \frac{1}{2^i - 1} \sum_{j=0}^{i-1} m_{i-j}\gamma_j, \ \text{ with } \ m_k = \sum_{n=-J}^{J+1} n^k \bar{a}_n \ \text{ and } \ \gamma_0 = 1 \tag{41}$$

and

$$\Gamma_i = \frac{1}{2^i} \sum_{j=0}^{i} \binom{i}{j} l_{i-j}\gamma_j, \ \text{ with } \ l_k = \sum_{n=-J}^{J+1} n^k \bar{b}_n \tag{42}$$

Straighforward integrations by part lead to

$$\alpha = -\frac{1}{2} Im(\gamma_2), \quad \beta = -\frac{\kappa Re(\Gamma_{J+3}) + Im(\Gamma_{J+3})}{(J+3)(J+2)Re(\Gamma_{J+1})} \ \text{ and } \ \kappa = -\frac{Im(\Gamma_{J+1})}{Re(\Gamma_{J+1})} \tag{43}$$

The numerical values found for $J = 2, 4$ and 6 are listed in the following table. They all agree with the values estimated from the Fourier representation of the identities (38).

	J=2	*J=4*	*J=6*
α	-0.164	-0.089	-0.076
β	-0.077	-0.089	-0.103
κ	-0.774	-1.168	-1.463

In most applications, the signal to be analyzed is real valued. In the present work and Ref.[10], the complex wavelet representation provides a redundant description of the signal. The previous result helps in interpreting this redundancy since, using the Taylor expansion of a one dimensional field, we can estimate the real

Figure 5: Original picture: "lady256"

and imaginary parts of the coefficients c_k^j in (7) as

$$\begin{cases} Re(c_k^j) \simeq 2^{\frac{-j}{2}} f(x_{j,k}) \\ Im(c_k^j) \simeq \frac{\alpha}{2^{\frac{3}{2}j+1}} f''(x_{j,k}) \end{cases} \quad \text{with } x_{j,k} = \frac{2k+1}{2^{j+1}}. \tag{44}$$

5. A SHARPENING ENHANCEMENT ALGORITHM

Let us now turn to the bi-dimensional case. The real and imaginary parts of the scaling function (25) are

$$\begin{cases} \Theta(x,y) = h(x)h(y) - g(x)g(y) \simeq G(x,y) \\ \Psi(x,y) = h(x)g(y) + g(x)h(y) \simeq \alpha \triangle G(x,y) \end{cases} \tag{45}$$

where $G(x,y)$ denotes the real smoothing kernel $h(x)h(y)$. We see that in one hand the real part of the 2-d scaling function is close (because $\alpha^2 << 1$) to the smoothing kernel $G(x,y)$ while, on the other hand, the imaginary part is proportional to the Laplacian of $G(x,y)$: $\Psi(x,y)$ is thus the "Marr wavelet" associated with $\Theta(x,y) \simeq G(x,y)$.

The simultaneous presence of a smoothing kernel and its Laplacian in the complex scaling function can be exploited to define some elementary operations on the wavelet coefficients. Since the real and imaginary parts of the wavelet transform coefficients of some *real* image correspond to the convolution of the original field with the real part and the imaginary part respectively of $\Phi_{j,m,n}(x,y)$, we then have access to the (multiscaled) smoothed Laplacian of the image.

Let us consider an image, *i.e* a real matrix $I_{m,n}$, and the bi-dimensional (complex valued) field $f(x,y)$ defined by the expansion (29) with $c_{m,n}^{j_{max}} = I_{m,n} \in \mathbb{R}$.
The field $f(x,y)$ is a particular point in the space $R_{j_{max}}$ defined as the set of all fields constructed with real scaling coefficients at scale j_{max}. We denote by P_R the orthogonal projector on this space; it is simply

defined by keeping the real part of the scaling coefficients only:

$$P_R\Big(\sum_{m,n}(h_{m,n}^{j_{max}} + ig_{m,n}^{j_{max}})\Phi_{j_{max},m,n}(x,y)\Big) = \sum_{m,n} h_{m,n}^{j_{max}}\Phi_{j_{max},m,n}(x,y) \tag{46}$$

Let us now define a smoothing operator $Z: R_{j_{max}} \rightarrow R_{j_{max}+1}$ by the inverse wavelet transform with the real part of the SDW filters only. The image Zf is twice larger than the original image, without spurious high-frequency components. Then, we can verify that the complex wavelet decomposition $W_1 Zf$ gives, in the imaginary part of the scaling coefficients, a good estimate of the Laplacian of $I_{m,n}$. In other words, $I(x,y) = Zf(x,y)$ is a good approximation of a *real* field in $R_{j_{max}+1}$.

For the sake of illustration, we consider the image displayed on Figure 5. Figure 6 shows the upper left corner of the image resulting from the application of Z, and Figure 7 displays the imaginary part of the scaling coefficients of $W_1 Zf$. As expected, the zero-crossings in this picture correspond to the edges in the original image.

Let us now consider a N-level decomposition of Zf. The real and imaginary parts of the coefficients c_{k_1,k_2}^l ($l = j_{max} - N$) can be written as ($*$ denotes the usual convolution operator)

$$\begin{cases} h_{k_1,k_2}^l = Re(c_{k_1,k_2}^l) = 2^l I(x,y) * G(2^l x - k_1, 2^l y - k_2) \\ g_{k_1,k_2}^l = Im(c_{k_1,k_2}^l) = -\frac{\alpha}{2^l}\triangle I(x,y) * G(2^l x - k_1, 2^l y - k_2) \end{cases} \tag{47}$$

To illustrate this result, we consider the sharpening operator, $f \rightarrow \tilde{f} = f - \rho\triangle f$. It can be implemented at the finest resolution scale through (we normalize the initial data such that $j_{max} = 0$)

$$c_{m,n}^{j_{max}} \rightarrow \tilde{c}_{m,n}^{j_{max}} = c_{m,n}^{j_{max}} + \frac{\rho}{\alpha} g_{m,n}^{j_{max}} \tag{48}$$

followed by the projection of this enhanced complex field on $R_{j_{max}}$:

$$\tilde{I}(x,y) = P_R\Big(\sum_{m,n}\tilde{c}_{m,n}^{j_{max}}\Phi_{j_{max},m,n}(x,y)\Big) = \sum_{m,n}\tilde{h}_{m,n}^{j_{max}}\Phi_{j_{max},m,n}(x,y) \tag{49}$$

This algorithm can easily be generalized to obtain a non-linear multiscale enhancement by considering a N level decomposition of Zf and by applying the adapted enhancement

$$c_{m,n}^j \rightarrow c_{m,n}^j + \frac{\rho_j}{2^{2(j_{max}-j)}\alpha} g_{m,n}^j \tag{50}$$

at any coarse scale with different sharpening parameter ρ ($\rho \rightarrow \rho_j$). The coefficients $c_{m,n}^j$ are induced by the synthesis process, whereas the coefficients $g_{m,n}^j$ are calculated during the decomposition process.

The Figure 8 shows an example of such processing with $SDW2$ and $N = 4$. In comparison with the original image (Fig.4), the local contrast has been improved significantly. Other tests of this algorithm have been performed on more challenging images, *i.e.* low-resolution and low-contrast mammographic images[9].
Let us mention that other efficient multiscale sharpening transformations have been proposed in the recent past[19,20]. The main difference here in the present work is the orthogonality property of the SDW transform. We recall that the SDW bases are not derived from a representation that allows specific enhancements. On the contrary, we have shown that the Laplacian was inherent to this particular orthogonal basis.

6. SHRINKAGE AND PHASE

Other important non-linear transformations in image processing are regression modeling and denoising. Mostly advocated by Donoho and Johnstone[15], the wavelet regression estimators, based on orthogonal multiresolution bases and the shrinkage of the empirical wavelet coefficients, provide near-optimal estimates of the true signal. Apart from the choice of the basis, the wavelet regression technique suggested by the authors of the Ref.[15] relies on the definition of the thresholding rule (hard or soft) and the selection of the appropriate threshold (optimal or universal). Based on the amplitude of the wavelet coefficients, this regression estimator can be directly implemented on the complex coefficients.

Let us define first a general *shrinkage* operation. From the empirical expansion

$$f_0(x,y) = \sum_{m,n} I_{m,n} \Phi_{j_{max},m,n}(x,y) \tag{51}$$

we consider the field

$$\tilde{f}_0(x,y) = \sum_{m,n} \tilde{I}_{m,n} \Phi_{j_{max},m,n}(x,y) \tag{52}$$

with

$$\tilde{I} = (\mathcal{W}_N^{-1}\, \mathcal{T}\, \mathcal{W}_N)\, I \tag{53}$$

where the *shrinkage operator* $\mathcal{T}$,

$$\mathcal{T}(\{c_{m,n}^{j_{max}-N}, \mathbf{d}_{j_{max}-N,m,n}, \dots \mathbf{d}_{j_{max}-1,m,n}\}) = \left(c_{m,n}^{j_{max}-N}, \eta(\mathbf{d}_{j_{max}-N,m,n}), \dots, \eta(\mathbf{d}_{j_{max}-1,m,n})\right) \tag{54}$$

is defined by

$$\eta(\mathbf{d}) = \left(\eta_0(|d^0|)\frac{d^0}{|d^0|}, \eta_1(|d^1|)\frac{d^1}{|d^1|}, \eta_2(|d^2|)\frac{d^2}{|d^2|}\right), \quad \text{with } \eta_i \colon \mathbb{R}^+ \to \mathbb{R}^+ \tag{55}$$

This operator only modifies the amplitude of the wavelet coefficients; the phases are preserved.

Given the complex wavelet coefficients $\{c_{m,n}^{j_{max}-N}, \mathbf{d}_{j_{max}-N,m,n}, \dots \mathbf{d}_{j_{max}-1,m,n}\}$ associated with f_0, we define the space of all the fields $f(x,y)$ such that

$$f(x,y) = \sum_{k_1,k_2} c_{k_1,k_2}^{j_{max}-N}\, \Phi_{l,k_1,k_2}(x,y) + \sum_{i=0}^{2} \sum_{j=1}^{N} \sum_{k_1,k_2} f_{j_{max}-j,k_1,k_2}^{i}\, \Psi_{j_{max}-j,k_1,k_2}^{i}(x,y) \tag{56}$$

with

$$Arg(f_{j,m,n}^{i}) = Arg(d_{j,m,n}^{i}), \quad \forall i,j,m,n \tag{57}$$

We call this space the *isophase space* $\Gamma_{j_{max}}$. Any shrinkage operator $\mathcal{T}$ maps f_0 towards some point in $\Gamma_{j_{max}}$. We denote by P_Γ the orthogonal projector onto this space. This operator is simply given by the orthogonal projections (*i.e.* the closest point) of each complex wavelet components $f_{j,m,n}^{i}$ on the half-line defined by the phase $Arg(d_{j,m,n}^{i})$. Notice that this projection can naturally "kill" a coefficient for which the closest point on the half-line (defined by the phase) is the origin in the complex plane.
Of course, the initial empirical field f_0 and the "shrunk field" $\tilde{f}_0$ (whatever the shrinkage operator) belong to $\Gamma_{j_{max}}$. The isophase space and the space $R_{j_{max}}$ are both convex spaces and the intersection $\Gamma_{j_{max}} \cap R_{j_{max}}$ contains, at least, the field f_0 (see Fig. 9).

Let us now consider the sequence of real images $I_{m,n}^{l}$ defined by

$$\sum_{m,n} I_{m,n}^{l}\, \Phi_{j_{max},m,n}(x,y) = \left(P_R P_\Gamma\right)^{l} P_R \tilde{f}_0 \tag{58}$$

Well-known theorems[21] prove the convergence of this sequence to a point in $\Gamma_{j_{max}} \cap R_{j_{max}}$, as $l \to \infty$.

As a first example of shrinkage, we take the functions $\eta_i(x) = 0$ in Eq.(55). This shrinkage is nothing but the usual projection (denoted by P_{V_N}) of $f_0 \in V_{j_{max}-N}$ onto the approximation space $V_{j_{max}-N}$. A typical example of such projection is shown on Figure 10. Starting from this "shrunk representation" of the original image and using the isophase space associated with the original image (see Figure 5), the iterative projections on the convex $\Gamma_{j_{max}}$ and $R_{j_{max}}$ lead to $I^{30}_{m,n}$ (Fig. 9) and $I^{1000}_{m,n}$ (Fig. 10). As well illustrated in the present example, the "wavelet phase reconstruction algorithm" restores the edges and small features blurred by the shrinkage. During the alternate projections, the percentage of phase *effectively* used to restore the non-vanishing amplitudes of the wavelet coefficients, gradually increases from 50% (first iteration) to 75% (30 iterations) and then 90% (1000 iterations and more).
The choice of the SDW wavelet and the definition of the shrinkage (*i.e.* $\tilde{f}_0$) apparently have no effect on the limit; however, they obviously affect the speed of convergence.
The complete characterization of $\Gamma_{j_{max}} \cap R_{j_{max}}$ is still an open problem. However, in one dimension, some prior investigations tend to demonstrate the uniqueness of f_0 in this space. Let us sketch an heuristic proof. We first observe that the complex conjugate of the wavelet, $\bar{\psi}$, has a non-vanishing projection on V_0 and on all the "details spaces" $W_{j\geq 0}$

$$\bar{\psi}(x) = \sum_{k=-2J}^{2J} \beta_k \, \varphi_{0,k}(x) + \sum_{j\geq 0} \sum_k \beta^j_k \, \psi_{j,k}(x) \tag{59}$$

The coefficients $\beta_k = -\beta_{-k}$ (non vanishing for $|k| = 1, 2, \ldots 2J$) and β^j_k can be acurately computed through a cascade algorithm. Any function in $\Gamma_{j_{max}} \cap R_{j_{max}}$ can be written as $f_0(x) + \delta(x)$ where

$$\delta(x) = \sum_{j=1}^{N} \sum_k \eta^i_{j_{max}-j,k} \, d^i_{j_{max}-j,k} \; \psi_{j_{max}-j,k}(x) \tag{60}$$

with $\eta^i_{j_{max}-j,k} \geq -1$. Assuming that $f_0(x) + \delta(x)$ is mostly a *real*-valued field for any small values of $\eta^i_{j_{max}-j,k}$, the reality condition $\delta(x) = \bar{\delta}(x)$ leads to an over-determined system of constraints on the η's since the expansion in Eq.(60) is *only* in terms of the orthogonal wavelets at a finite number of different scales: the reality condition together with the expansion of $\bar{\psi}$ put severe constraints on $\delta(x)$ and $\delta(x) = 0$ is the unique solution. More carefull analysis of this statement is presently under investigation.

An other typical example of shrinkage is the *soft-thresholding* function used in wavelet-regression:

$$\eta_i(t) = (t - t_i) \, I(t > t_i), \quad t \in \mathbb{R}^+ \tag{61}$$

where $I(x)$ is the indicator function. The thresholds t_i are the most important parameters of this regression method. The *universal thresholds*, that lead to a noise-free estimate, are defined as $t_i = \sqrt{2log(n^2)}\sigma_i$, n^2 being the size of the image and σ_i the noise variance directly estimated from the modulus of the wavelet coefficients $d^i_{j_{max}-1,m,n}$. A simple estimation is given[15] by $\hat{\sigma}_i = median(|d^i_{j_{max}-1,m,n}|)/0.6745$.
In most applications where noise is important (see Figure 13), the usual wavelet regression techniques tend to underfit the true signal by shrinking too many coefficients[22]. The same observation is made with the SDW when we consider the real image produced by the scaling coefficients of $P_R\tilde{f}_0$ (see Fig. 14). However, in many experiments we noticed that local artefacts in the universal estimate were in correspondence with transients in the imaginary part of the scaling coefficients of $\tilde{f}_0$. This observation leads us to consider the improvement

of the universal estimate by using the information contained in the phase of the wavelet coefficients and left untouched by the shrinkage operation.
Figure 15 and Fig.16 display the resulting image after 30 and 1000 iterations of alternate projections respectively. Here again, the restoration of the amplitudes of the wavelet coefficients is such that coherent structures of the image are restored firstly. Noise is also induced during the projections but, quite remarkably, major part of the noise introduced with the phase (we use the isophase space of the noisy image in P_{Γ}) is immediately pumped out with the elimination of imaginary part of the scaling coefficient (in P_R).

One-dimensional simulations have also shown that it was possible to improve the "wavelet phase-only reconstruction" algorithm by defining an isophase space from the statistical results of Donoho and Johnstone. This amounts to interpret somewhat differently their results: the threshold being chosen (*i.e* defined from the *a priori* knowledge of the noise content in the signal), the wavelet coefficients of modulus less than the threshold are set to zero which means that the corresponding phases are *undefined*. In other words, no relevant information for describing the true signal is encoded in those phases. However, the phase of the remaining coefficients of modulus greater than the threshold are meaningful and we claim that those phases and those phases only contain all the available informations for describing the true signal. This subset of phases defines a new isophase space $\tilde{\Gamma}_{j_{max}} \subset \Gamma_{j_{max}}$. Various simulations have shown that using this new isophase space in the alternate projections (58) gives an effective shrinkage of the empirical wavelet coefficients similar to a compromise between the "hard "and "soft" thresholdings. This "phase reconstruction algorithm" improves significantly the initial estimate by adapting the thresholding rule to the coherence of the signal.In this "holographic" interpretation of the shrinkage techniques, the wavelet coefficient amplitude doest not carry pure information about the true signal but rather weights the information contained in the phase of the coefficient.

7. CONCLUSION

After a review of the construction of the Symmetric Daubechies Wavelets, we have described a simple multiresolution processing algorithm based on the inherent Laplacian kernel in this type of orthogonal bases. Beside this operation which acts on the scaling coefficients only, we have discussed the importance of the phase in the wavelet coefficients. Most information of a real signal is indeed encoded in this phase of the wavelet coefficients. We note that, despite the orthogonality of the present wavelet bases, the redundancy of the complex representation of real signals is utilized. In fact, both algorithms (enhancement and restoration) emphasize the role of the phases in this type of complex multiresolution decompositions.
The phase representation of images is quite appealing. It is worth mentionning that experiments in physiology also demonstrate the crucial role of both a redundant multiresolution signal processing[23,24] and the phase information[25,26] in the Human Vision System. Quite remarkably, the symmetry condition, which is required in image analysis for very practical reasons, leads to multiresolution representations that seem to be of main relevance in Nature[27]. Far from being an immediate model for the visual perception, the complex symmetric Daubechies wavelets suggest,at least, new directions of investigation in image processing like, for instance, the use of complex convolutions in layered neural networks for pattern recognition.

8. ACKNOWLEDGMENTS

The author wishes to thank L. Gagnon and M. Mayrand for their precious collaboration, and Stéphane Mallat for discussions about the "phase reconstruction" algorithm. This work was supported in part by the Natural Sciences and Engineering Research Council (NSERC) of Canada.

8. REFERENCES

1. D. Marr, *Vision*, W.H. Freeman, San Francisco, 1982.
2. D. Marr and E. Hildreth, "Theory of edge detection", Proc. Royal So. London, vol.207, p.187-217, 1980.
3. J. Canny, "A computational approach to edge detection", IEEE Trans. Pattern Anal. Machine Intell., vol.8, p.679-698, 1986; I.D.G. Macleod, "On finding structures in picture" in Picture Language Machines, S. Kaneff ed., Academic Press, New York, p.231, 1970.
4. S. Mallat, "Zero-crossings of a wavelet transform", IEEE Trans. Info. Theory, vol.37, p.1019-1033, 1991.
5. S. Mallat and S. Zhong, "Characterization of signals from multiscale edges", IEEE Trans. Patt. Anal. Machine Intell., vol.14, p.710-732, 1992.
6. W. Lawton, "Applications of Complex Valued Wavelet Transforms to Subband Decomposition", IEEE Trans. on Signal Proc., vol.41, p.3566-3568, 1993.
7. J.M. Lina and M. Mayrand, "Complex Daubechies Wavelets", App. Comp. Harmonic Anal., vol.2, p.219-229, 1995.
8. L. Gagnon and J.M. Lina, "Symmetric Daubechies wavelet and numerical solution of NLS equations", Jour. Phys. A, vol.27, p.8207-8230, 1994.
9. B. Belzer, J.M. Lina and J. Villasenor, "Complex linear phase filters for efficient image coding", to be published in IEEE Trans. on Signal Proc., 1995; L. Gagnon, J.M. Lina and B. Goulard, "Sharpening Enhancement of Digitalized Mammograms with Complex Symmetric Daubechies Wavelets", 17^{th} IEEE and EMBS Conf., Montreal, Sept. 1995.
10. J.-M. Lina, "From Daubechies to Marr", ANS-PhysNum Report 20, Univ. of Montreal, March 1995.
11. A.V. Oppenheim and J.S. Li, "The importance of phase in signals", Proc. IEEE, vol.69, p.529-541, 1981.
12. M. Hayes, "The reconstruction of a multidimensional sequence from the phase or magnitude of its Fourier transform", IEEE Trans. ASSP, vol.30, p.140-154, 1982.
13. A. Levi and H. Stark, "Signal restoration from phase by projections onto convex sets", J. Opt. soc. Am., vol.73, p.810-822, 1983.
14. R. De Vore and B. J. Lucier, "Fast wavelet techniques for near-optimal image processing", Proc. 1992 IEEE Military Commun. Conf., IEEE Communications Soc., NY 1992.
15. D. Donoho and I. Johnstone, "Adapting to unknown smoothness via wavelet shrinkage", to be published in J. Amer. Statist. Assoc., 1995 (and reference therein).
16. I. Daubechies, "Orthonormal bases of compactly supported wavelets", Comm. Pure Appl. Math., vol.41, p.909-996, 1988.
17. I. Daubechies, *Ten lectures on Wavelets*, SIAM, CBMS Series, 1992, see page 253.
18. D. Pollen, "$SU_I(2, F[z, 1/z])$ for F a subfield of C", Comm. Purre Appl. Math., vol. 45, p.485, 1990.
19. A. F. Laine, S. Schuler, J. Fan and W. Huda, "Mammographic Feature Enhancement by Multiscale Analysis", IEEE Transactions on Medical Imaging vol. 13, pp. 725-740, 1994.
20 J. Lu, D. M. Healy Jr. and J. B. Weaver, "Contrast Enhancement of Medical Images Using Multiscale Edge Representation", SPIE vol. 2242 Wavelet Applications, pp. 711-719, 1994
21. D.C. Youla and H. Webb, "Image restoration by the method of convex projections", IEEE Trans. on Medical Imaging, vol. 1 (2), p.81-94, 1982.
22. G. P. Nason, "Wavelet regression by cross-validation", Tech. Report 447. Dept. of Statistic, Stanford (April 1994), and references therein.
23. J. Daugman, "Uncertainty relation for resolution in space, spacial frequency, and orientation optimized by two-dimentional visual cortical filters", J. Opt. Soc. Am. A, vol. 2 (7), p.1160, 1985.
24. S. Mallat, "Multifrequency channel decomposition of images and wavelet models", IEEE Trans. ASSP. vol. 37 (12), p. 2091, 1989.
25. D.A. Pollen and S. Ronner, "Phase relationships between adjacent simple cells in the visual cortex", in *Science*, 212, p.1409, 1981.
26. A. Burgess and H. Ghandeharian, "Visual signal detection. I. Ability to use phase information", J. Opt. Soc. Am., vol.1, p.900-905, 1984.
27. M. Concetta Morrone and D.C. Burr, "Feature detection in human vision: a phase-dependent energy model", Proc. R. Soc. Lond. B235, p.221, 1988

Figure 6: Z(lady256) with SDW2 (upper left corner)

Figure 7: Imaginary part of the scaling coefficients of $W_1 Z$(lady256)

Figure 8: Processed image with N=4 and SDW2

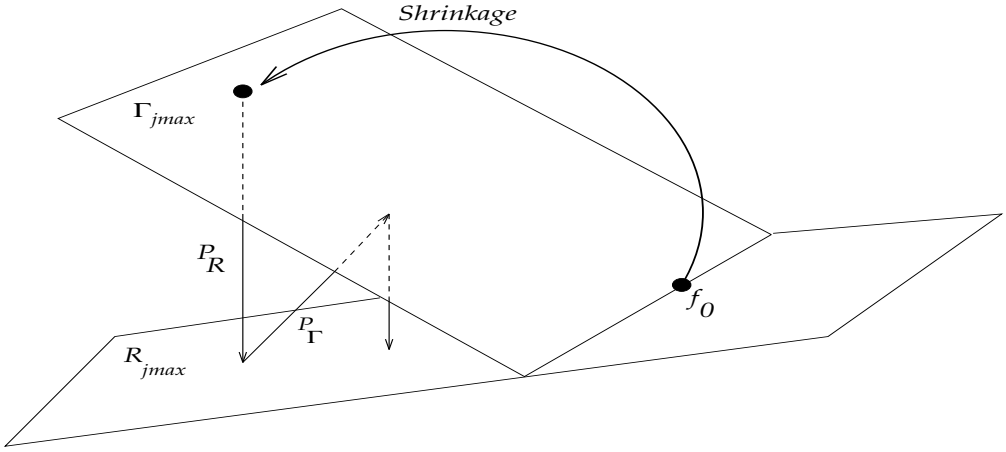

Figure 9: Phase reconstruction by alternating projections on convex spaces $\Gamma_{j_{max}}$ and $R_{j_{max}}$

Figure 10: $P_R \circ P_{V_4}$(lady256)

Figure 11: POCS with 30 iterations (4 levels)

Figure 12: POCS with 1000 iterations (4 levels)

Figure 13: Noisy lady256, (Gaussian random noise, psnr = 10db)

Figure 14: visu-shrinkage of the noisy lady256, (SDW2, 4 levels)

Figure 15: POCS with 30 iterations from the visu-shrinkage (SDW2, 4 levels)

Figure 16: POCS with 1000 iterations from the visu-shrinkage (SDW2, 4 levels)